Comm. Korean Math. Soc. **16** (2001), No. 1, pp. 137–152

COMPUTATION OF FREE-SURFACE FLOWS DUE TO PRESSURE DISTRIBUTION

JACK ASAVANANT, MONTRI MALEEWONG, AND JEONGWHAN CHOI

ABSTRACT. Steady two-dimensional flows due to an applied pressure distribution in water of finite depth are considered. Gravity is included in the dynamic boundary condition. The problem is solved numerically by using the boundary integral equation technique. It is shown that, for both supercritical and subcritical flows, solutions depend on three parameters: (i) the Froude number, (ii) the magnitude of applied pressure distribution, and (iii) the span length of pressure distribution. For supercritical flows, there exist up to two solutions corresponding to the same value of Froude number for positive pressures and a unique solution for negative pressures. For subcritical flows, there are solutions with waves behind the applied pressure distribution. As the Froude number decreases, these waves diminish when the Froude numbers approach the critical values.

1. Introduction

Efforts to analyze the hydrodynamical characteristics of free-surface flow with surface-disturbance have been divided primarily between theoretical and experimental considerations. In ship hydrodynamics, the concerns are mostly on the understandings of wave resistance corresponding to the moving vehicles.

In the paper, we consider a steady nonlinear flow due to an applied pressure distribution over a portion of the free surface. The assumption of steadiness is based upon the fact that we can always choose the appropriate moving frame of reference with the flow. This flow configuration can be served as a model of moving vehicles such as hovercraft in a canal. It may

Received April 12, 2000. Revised September 5, 2000.

2000 Mathematics Subject Classification: 76Mxx.

Key words and phrases: pressure distribution, wave.

This research was supported in parts by the Thailand Research Fund and Chulalongkorn University' Research Division and Kosef 981-0106-037-2. The authors wish to thank the National Electronic and Computer Technology Center-NECTEC for allowing some massive calculations to perform on their high performance computer.

also be viewed as an inverse method of solution to the classical ship-wave problem.

The classical linearized version of two-dimensional model in water of infinite depth was discussed in detail by Lamb [1]. He showed that for certain span length of pressure distribution (in relation with the Froude number) the motion possesses no drag and the free surface profile is symmetric. Schwartz [2] reformulated the problem as a nonlinear integral equation and solved it numerically. His numerical results show that, for certain values of the Froude number, nonlinear theory produces a drag-free solution while linear theory does not. In the case of water of finite depth, Von-Kerczek and Salvesen [3] investigated the problem by using finite difference techniques. They calculated by placing a network of mesh points all over the fluid domain. Asavanant and Vanden-Broeck [4] proposed a model for flows past a surface-piercing object in water of finite depth and formulated the problem as an system of nonlinear integrodifferential equations.

Here we consider the fluid domain of finite depth. The conditions of incompressibility and irrotationality of the fluid motion imply the existence of the potential function and the stream function. The fluid domain in the physical plane is transformed onto the complex plane. Bernoulli equation is applied on the free surface while we assume no flow across the bottom boundary. We satisfy the bottom condition by using Schwartz reflection principle. The problem is solved numerically by boundary integral equation method based on Cauchy's integral formula. It is found that solutions depend on three parameters: the Froude number F, the magnitude of pressure distribution ϵ, and the span length of pressure distribution. For supercritical flows, there exists up to two solutions when $\epsilon > 0$ and only one solution when $\epsilon < 0$. For subcritical flows, the solutions are characterized by a train of nonlinear waves on the downstream free surface. These waves vanish as the Froude numbers approach their critical values. This behavior of subcritical solutions is found to be different from the case of surface-piercing object (Asavanant and Vanden-Broeck, [4]).

In section 2, we formulate the problem by using the complex function theory and construct an integral equation involving the flow variables on the free surface. Numerical procedure is introduced in section 3. In section 4, we present and discuss the results for both supercritical and subcritical flows. Concluding remarks and further suggestions are given in section 5.

2. Mathematical Formulation

We consider the steady two-dimensional irrotational flow of an inviscid and incompressible fluid in the domain bounded below by a rigid bottom

and above by a free surface as shown in Figure 1. We choose Cartesian coordinates with the x-axis along the undisturbed free surface at infinity and the y-axis directed vertically upwards through the symmetry line of the applied pressure distribution. Gravity is acting in the negative y-direction. Let the velocity components in the x- and y- directions be denoted by u and v respectively. The flow approaches a uniform velocity U and uniform depth H as $x \to -\infty$.

Let ϕ and ψ denote the velocity potential and the stream function. The complex potential function is defined by $f = \phi(x, y) + i\psi(x, y)$. Without loss of generality, we choose $\phi = 0$ at the point on the free surface where maximum pressure is applied. Free surface is a streamline on which we require $\psi = 0$. The bottom boundary defines another streamline on which $\psi = -UH$. On the free surface, the Bernoulli equation yields

$$q^2/2 + gy + p/\rho = U^2/2 + p_0/\rho. \tag{1}$$

Here q, g, ρ, p, and p_0 represent the magnitude of the velocity, the acceleration of gravity, the fluid density, the applied pressure on the free surface, and the atmospheric pressure respectively.

We choose U as the unit of velocity and H as the unit of length. Then (1) becomes, in dimensionless form,

$$q^2 + (2/F^2)y - \tilde{p} = 1 \tag{2}$$

where $\tilde{p} = 2(p - p_0)/\rho U^2$ and F is the Froude number defined by

$$F = U/\sqrt{gH}. \tag{3}$$

By the choice of our dimensionless variables, the free surface and the bottom define the streamline $\psi = 0$ and $\psi = -1$ respectively. In the plane of complex potential f, the flow domain is $D = \{(\phi, \psi) | -\infty < \phi < \infty, -1 < \psi < 0\}$. Let us introduce the complex velocity $\zeta = \frac{df}{dz} = u - iv$ where $z = x + iy$. The kinematic boundary condition on the bottom can be described by

$$\mathrm{Im}\zeta = 0 \quad \text{on} \quad \psi = -1. \tag{4}$$

We now define an analytic function $\xi = u - iv - 1$ in the fluid domain. Here ξ is real on the bottom $\psi = -1$. We satisfy (4) by reflecting the flow field in the physical z-plane about the line $y = -1$ (also in the complex f-plane about the line $\psi = -1$). Let Ω and $\overline{\Omega}$ denote the fluid domain in the z-plane and its reflection. The function ξ can be extended to a function Ξ, which is analytic in $\Omega \cup \overline{\Omega}$ and is defined by

$$\Xi(z) = \begin{cases} \overline{\xi(\overline{z})} & , \quad z \in \overline{\Omega} \\ \xi(z) & , \quad z \in \Omega. \end{cases}$$

The overbar represents the complex conjugation of the function. The extended fluid domain in the complex f-plane is now a strip $-2 \leq \psi \leq 0$. Using the Cauchy's integral formula to the function Ξ, we get

$$\Xi = u - iv - 1 = -\frac{1}{2\pi i} \oint_{\Gamma} \frac{u(f') - iv(f') - 1}{f' - f} df'.$$

Here Γ is the negatively oriented contour consisting of the free surface, the reflection of the free surface, and the lines $x = -\infty$ and $x = +\infty$ joining the free surface and its reflection. Upon letting f approach the boundary $\psi = 0$ and taking the real part of the resulting expression, we obtain

$$u(\phi) - 1 = \frac{1}{\pi} \int_{-\infty}^{\infty} \frac{v(\phi')}{\phi' - \phi} d\phi' + \frac{1}{\pi} \int_{-\infty}^{\infty} \frac{v(\phi')(\phi' - \phi) + 2(u(\phi') - 1)}{(\phi' - \phi)^2 + 4} d\phi'. \tag{5}$$

We denote by $u(\phi)$ and $v(\phi)$ the velocity components in the x- and y-directions on the free surface $\psi = 0$. Using the identity

$$\frac{\partial x}{\partial \phi} + i \frac{\partial y}{\partial \phi} = \frac{1}{u - iv}, \tag{6}$$

the Bernoulli equation (2) can be written in terms of $u(\phi)$ and $v(\phi)$ as

$$u^2(\phi) + v^2(\phi) + \frac{2}{F^2} \int_{-\infty}^{\phi} \frac{v(\phi')}{u^2(\phi') + v^2(\phi')} d\phi' + \tilde{p} = 1 \ , -\infty < \phi < \infty. \tag{7}$$

In this study, we consider the pressure distribution in the form of

$$\tilde{p} = \begin{cases} \epsilon e^{1/(|\phi/\phi_0|^2 - 1)} & , \ |\phi| < \phi_0 \\ 0 & , \ \text{otherwise.} \end{cases} \tag{8}$$

Here ϕ_0 denotes the value of the potential function that determines the span length of the applied pressure distribution in the complex f-plane. The problem becomes of that finding $u(\phi)$ and $v(\phi)$ satisfying (5) and (6). This completes the formulation of our problem. Once $u(\phi)$ and $v(\phi)$ are determined, the shape of the unknown free surface can be found by numerically integrating the identity (6).

3. Numerical Procedure

The numerical procedure used in this paper essentially follows the one used by Asavanant and Vanden-Broeck [4]. To solve the system of equations (5) and (6), we truncate the domain of integration in (5) at a finite value. Thus we introduce the M mesh points

$$\phi_i = (i-1)E, \quad i = 1, 2, ..., M$$

where E is the discretization interval. The values of $u(\phi)$ and $v(\phi)$ are computed at the mid points

$$\phi_{i+1/2} = \frac{\phi_i + \phi_{i+1}}{2}, \quad i = 1, 2, ..., M-1.$$

The truncation of fluid domain is done subject to the requirement that the pressure distribution is applied on the free surface sufficiently far from the end points. The error due to this truncation can be estimated by comparing the solutions for different values of M and E.

We approximate the integral in (5) by using the trapezoidal rule with summation over ϕ_i. The singularity of the Cauchy principal value can be ignored, since it occurs symmetrically between the mesh points. We satisfy (5) at the midpoints

(9)

$$u_{i+1/2} - 1 = \frac{1}{\pi} \int_{\phi_1}^{\phi_M} v_i \left[\frac{1}{\phi' - \phi_{i+1/2}} \right] d\phi' + \frac{1}{\pi} \int_{\phi_1}^{\phi_M} \frac{v_i(\phi' - \phi_{i+1/2}) + 2(u_i - 1)}{(\phi' - \phi_{i+1/2})^2 + 4} \, d\phi'.$$

The Bernoulli equation (6) is satisfied at mesh points

$$u_i^2 + v_i^2 + \frac{2}{F^2} y_i + \tilde{p}_i = 1, \quad i = 1, 2, 3, ..., M. \tag{10}$$

Thus we obtain the $2M-1$ nonlinear algebraic equations for $2M$ unknowns u_i and v_i. The last equation is obtained by imposing the radiation condition $v \to 0$ as $\phi \to -\infty$, i.e.,

$$v_1 = 0. \tag{11}$$

It is convenient to write this system of nonlinear algebraic equations in the form

$$f_i(\eta_1, \eta_2, ..., \eta_{2M}) = 0, \quad i = 1, 2, ..., 2M \tag{12}$$

where $\{\eta_i\}_{i=1}^{M} = \{u_i\}_{i=1}^{M}$ and $\{\eta_i\}_{i=M+1}^{2M} = \{v_i\}_{i=1}^{M}$.

We solve (12) by Newton's method. That is, if $\eta_j^{(k)}$ is an approximation to the solution at the mesh point j for the k th iteration, the next approximation $\eta_j^{(k+1)}$ is obtained by

$$\eta_i^{(k+1)} = \eta_i^{(k)} - \Delta_i^{(k)}, \quad i = 1, 2, ..., 2M \tag{13}$$

where the corrections $\Delta_j^{(k)}$ is calculated from

$$\sum_{j=1}^{2M} \left[\frac{\partial f_i}{\partial \eta_j}\right]^{(k)} \Delta_j^{(k)} = f_i{}^{(k)}, \quad i = 1, 2, ..., 2M. \tag{14}$$

The Jacobians are determined by exact differentiation of (12). Let us define the span length L of the pressure distribution by

$$L = \int_{-\phi_0}^{\phi_0} \frac{u}{u^2 + v^2}\, d\phi \quad \text{on} \quad \psi = 0.$$

Thus it is equivalent to specify the value of either L or ϕ_0.

4. Numerical Results and Discussions

We use the numerical scheme described in the previous section to compute solutions for various values of F^2, ϵ, and L. It is found that the behaviors of solutions are qualitatively similar for different values of L. Thus it is sufficient to present numerical results for a fixed value of L. The numerical accuracy is achieved by increasing M while keeping E fixed and vice versa. In this section, we present and discuss numerical solutions for two different flow regimes: supercritical flows ($F > 1$), and subcritical flows ($F < 1$). It is found that supercritical solutions are characterized by exponential decaying behaviors at infinity. This means that solutions in this flow regime can never possess waves for downstream. On the contrary, subcritical solutions are characterized by a train of nonlinear waves at infinity. As we shall see later, there are certain critical values of the Froude number that the amplitude of these waves tends to zero. This implies that the flow possesses no drag which is of interest in practice.

(i) Supercritical Solutions

In this subsection, we set $L = 3$ throughout the discussion of supercritical flows. We found that the results are independent of M and E, within graphical accuracy, for $M \geq 129$ and $E \leq 0.2$. The solutions converge

rapidly after a few iterations. All results presented here were obtained with $M = 199$ and $E = 0.15$.

Following Vanden-Broeck and Keller [5], we define the amplitude parameter

$$\alpha = \frac{W}{H}. \tag{15}$$

Here W is the distance from bottom to maxima or minima of the free surface profile upon which the pressure distribution is applied.

When $\epsilon = 0$, the pressure is everywhere equal to the atmospheric pressure and uniform flow is always a solution for all values of the Froude number greater than one. Besides uniform flow solution, we recover the so-called 'solitary wave' solution. The exact expression of solitary wave solution can be derived from the weakly nonlinear analysis (Lamb [1]) as

$$y = (F^2 - 1)\mathrm{sech}^2\Big[\Big(\frac{3}{4(1+F^2)}\Big)^{1/2} x\Big], \quad -\infty < x < \infty.$$

Our numerical results have a root mean square error of 0.418 % in comparison with this exact solution. This constitutes a check on our numerical scheme.

The solution for $\epsilon \neq 0$ can be viewed as a perturbation of the solutions for $\epsilon = 0$. When $\epsilon = 0$, there are two branches of solutions: the uniform flow $\alpha = 1$ and the solitary wave solution which bifurcates from the uniform flow at $F^2 = 1$. When $\epsilon \neq 0$, the uniform flow is no longer a solution for any value of F^2. Therefore we can expect a perturbed bifurcation from $F^2 = 1$.

When $\epsilon > 0$, the solutions are characterized by $\alpha - 1 > 0$. Typical free-surface profiles are shown in Figure 2. In Figure 3, we present numerical values of F^2 versus $\alpha - 1$ for various values of ϵ. Solutions of this type can be viewed as perturbations of the branch of solutions with $\epsilon = 0$ which bifurcate from $F^2 = 1$. On these branches of solutions, there are two critical values $\tilde{F}_1^2$ and $\tilde{F}_2^2$ of F^2 such that, for each ϵ, there are no solutions for $F^2 < \tilde{F}_2^2$, two solutions for $\tilde{F}_2^2 < F^2 < \tilde{F}_1^2$, and one solution for $F^2 > \tilde{F}_1^2$. They can easily be seen in Figure 3: the critical values $\tilde{F}_2^2$ are the turning points, and the critical values $\tilde{F}_1^2$ are on the upper dashed curve. When $F^2 = \tilde{F}_1^2$, solutions approach the limiting configuration with 120^0 angle corner at the crest (this is known as Stokes' highest wave). These limiting configurations are characterized by the relation;

$$\alpha - 1 = \frac{1}{2}\left(1 - \frac{\epsilon}{e}\right)F^2. \tag{16}$$

The height of the crest increases progressively as F^2 increases on the upper branch of the curves and ultimately the free surface profile reaches the aforementioned limiting configuration as $F^2 \to \tilde{F}_1^2$. Figure 4 shows a comparison of flow profiles at the same value of F^2, on both the lower and upper portions of the curves in Figure 3, for $\epsilon = 0.1$.

The solutions for the case $\epsilon < 0$ can be viewed as perturbations of a uniform flow (i.e. they approach the uniform stream as $\epsilon \to 0$ for a fixed value of F^2). These branches of solutions extend from $F^2 = 1$ to $F^2 = \infty$ (see Figure 5). We expect that these branches can be extended to the subcritical regime ($F^2 < 1$) by allowing waves downstream. Solutions with waves will be considered in the next subsection.

(ii) Subcritical Solutions

Unlike supercritical solutions, subcritical solutions have a train of waves behind the applied pressure distribution and a net horizontal drag force exerted on that portion of the free surface. Due to the presence of waves, numerical solutions for the subcritical case are more difficult to obtain than those in the previous subsection. In this case, the results were obtained with $M = 199$ and $E = 0.065$. The occurrence of nonphysical small amplitude periodic disturbance had been detected on the upstream free surface when ϕ_0 (position of the pressure distribution) was chosen inappropriately inspite of the radiation condition. This can be avoided if ϕ_0 was slightly adjusted. An important physical quantity of interest is the wave drag defined by

$$D = \int p n_x ds.$$

Here n_x is the x-component of the outward unit normal vector to the free surface. Typical profiles for $L = 0.39$ and $L = 0.65$ are shown in Figure 6 for $\epsilon > 0$ and in Figure 7 for $\epsilon < 0$ when $F^2 = 0.25$.

When $\epsilon = 0$, uniform flow is always the solution in this case. Figure 8 shows that the amplitude A of the waves, defined as the difference between the levels of the successive crest and trough, decreases as F decreases. The wave amplitude ultimately becomes zero when the critical value F_{*1} of F is reached. If we decrease F further, the wave amplitude increases to its maximum value and then decreases monotonically to zero again at $F = F_{*2}$. In addition, the free surface, upon which the pressure distribution is applied, deforms into "two humps" as depicted in Figure 9. This cycle of behavior repeatedly occurs as the Froude number F reaches other critical

values. We conjecture that there are finitely many critical Froude numbers $0 < ... < F_{*2} < F_{*1} < 1$ such that drag-free solutions exist. In addition, there are "n humps" on the free surface for solutions with $F_{*n} < F < F_{*n-1}$. Some of these critical values F_{*i} of the Froude number for $L = 0.39$ and $\epsilon = 0.1$ are presented in Table 1. Similar behavior can be found for the steepness of the waves, defined as the difference of heights between a crest and a trough divided by the wavelength, and the wave drag as shown in Figures 10(a) and (b) respectively. In order to obtain numerical solutions for $F < F_{*3}$, it is necessary to have a finer mesh to resolve the smaller wavelengths. This requires an extensive use of computer time.

Free surface profiles for the case of $\epsilon < 0$ are found to be similar to those of $\epsilon > 0$. Except the reverse signs of the wave amplitude A, overall behaviors of the solutions are qualitatively similar to the case of $\epsilon < 0$. We therefore omit the presentation of these results.

5. Concluding Remarks

In this paper, we have investigated the problem of free-surface flows due to pressure distributions. It is discovered that, for supercritical flows, the solutions exhibit similar behaviors to those obtained by Asavanant and Vanden-Broeck [4] for flows past a surface-piercing object. However, fewer solutions are found in our problem since the free surface is not partially replaced by a rigid obstacle. For subcritical flows, there are finitely many critical values of the Froude number such that the amplitudes of the wave train vanish. These imply that the motion possesses no drag and is of interest to architectural design of the moving vehicle on the free surface. It is worthwhile noting that these subcritical solutions never possess limiting configurations in the form of Stokes' highest waves, which are in contrast to the results found by Asavanant and Vanden-Broeck [4].

When the effect of surface tension is considered in the problem in conjunction with gravity, the flow behaviors become more complicated and require further investigation. The authors are now studying the problem of gravity-capillary waves subject to the applied pressure distribution in the fluid of finite depth. Preliminary results [6] show that limiting configurations in the form of "trapped bubbles" occur on the free surface. This phenomenon was first discovered by Kinnersly [7].

F_{*1}	0.1897
F_{*2}	0.1414
F_{*3}	0.1204
F_{*4}	0.1025

Table 1. Critical values $F*$ of Froude number for $L = 0.39$ and $\varepsilon = 0.1$

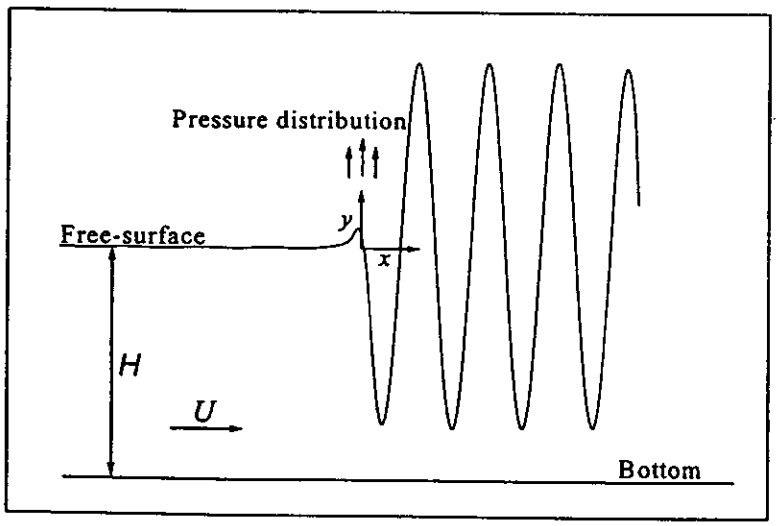

Figure 1

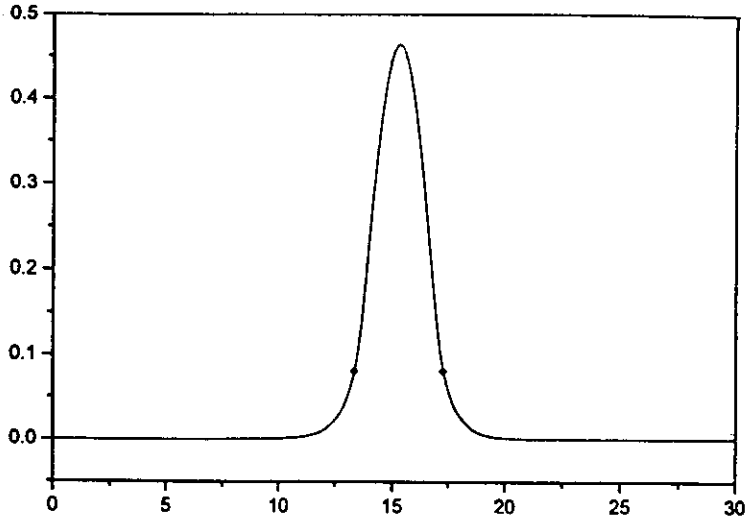

Figure 2

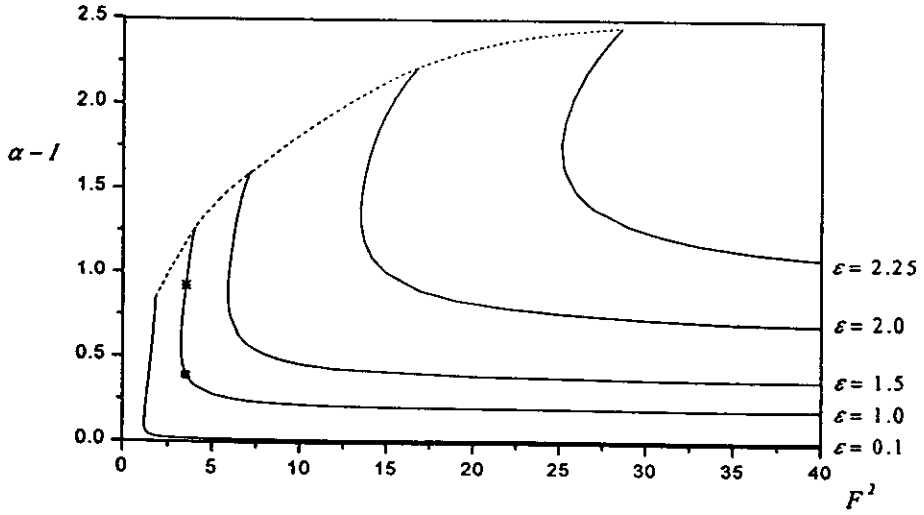

Figure 3

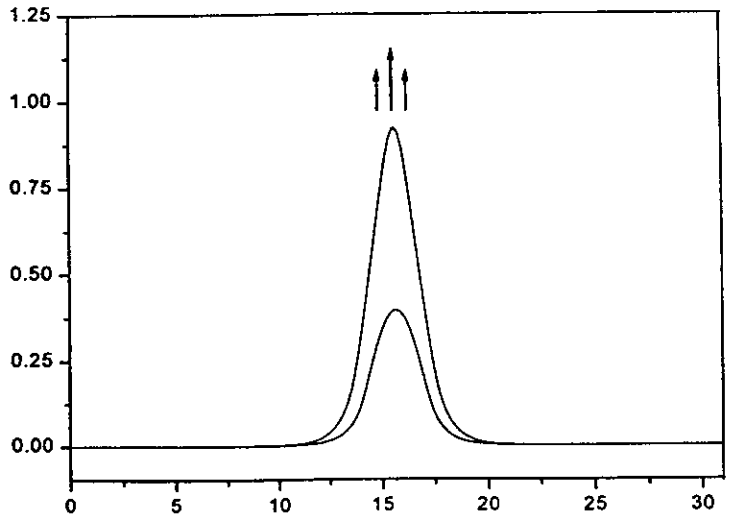

Figure 4

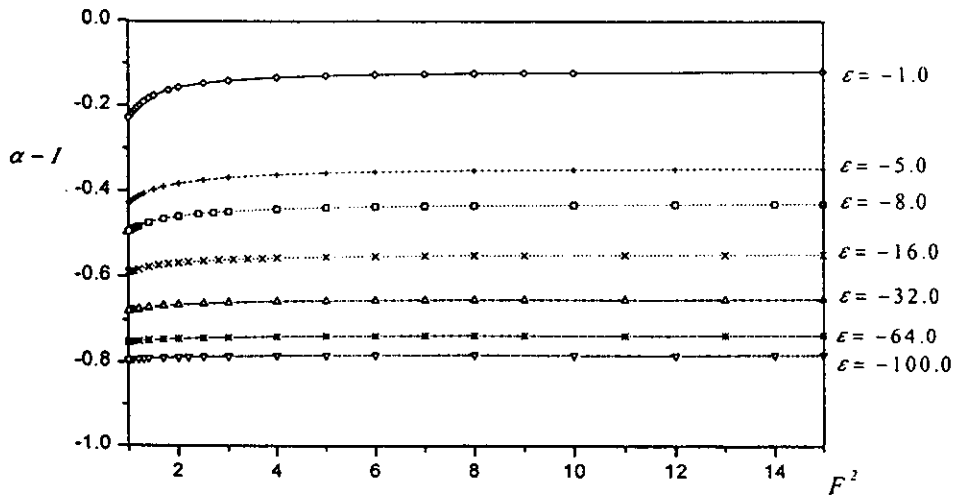

Figure 5

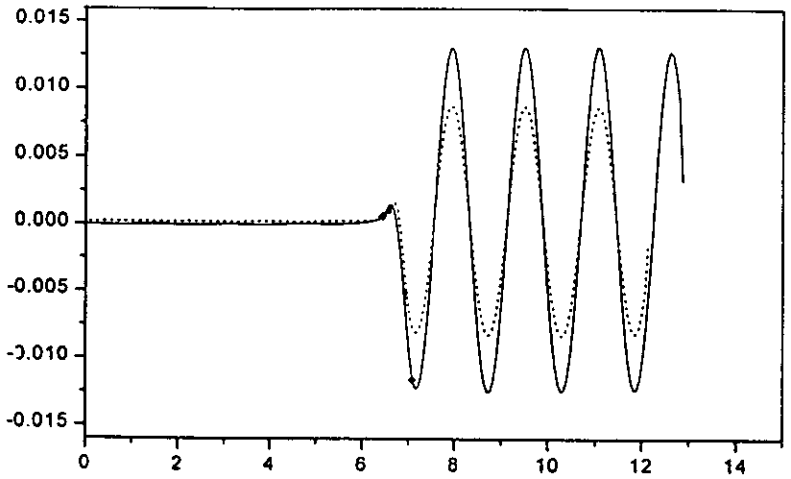

Figure 6

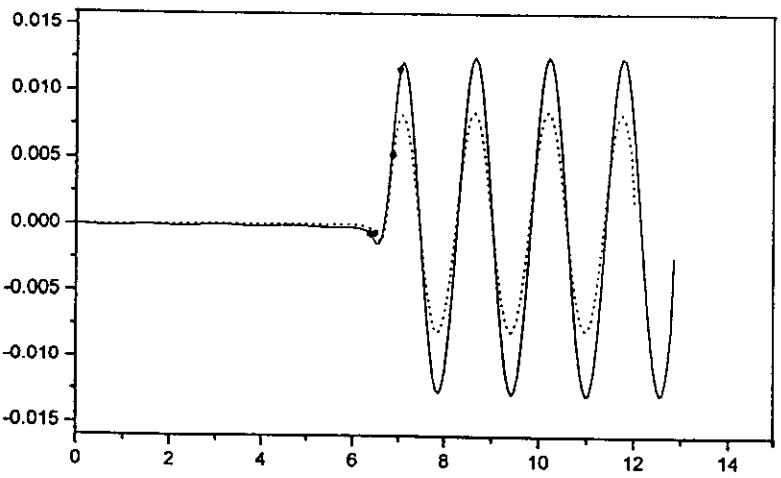

Figure 7

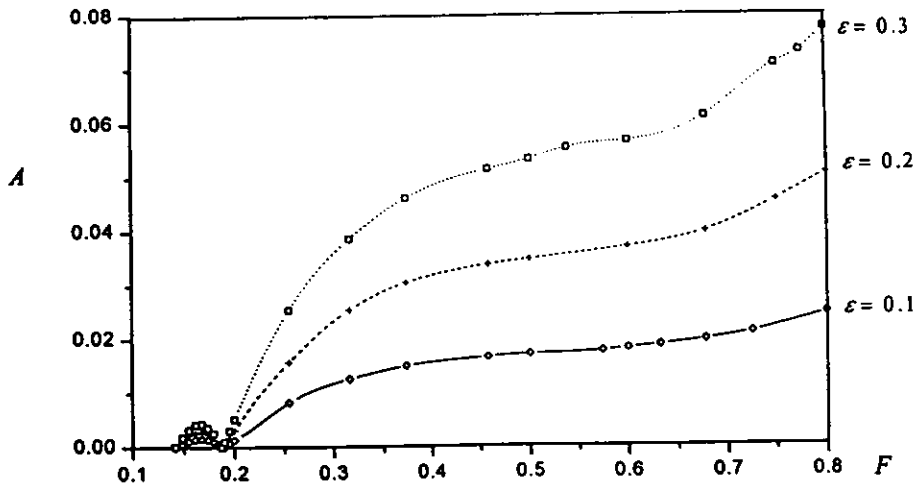

Figure 8

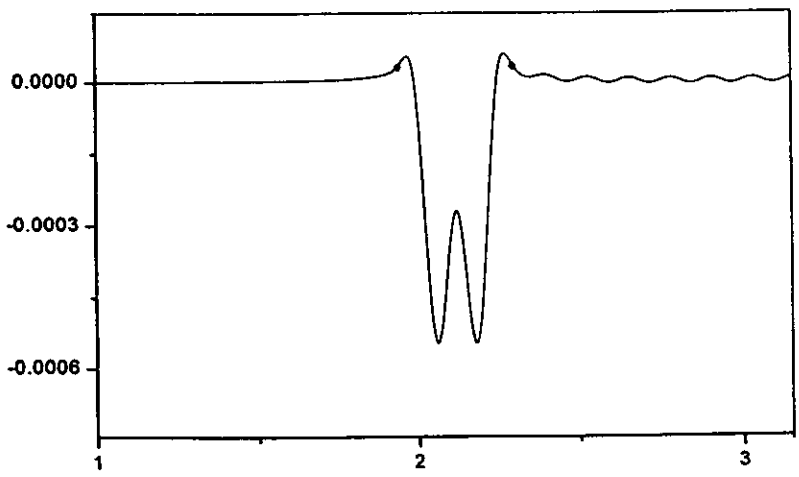

Figure 9

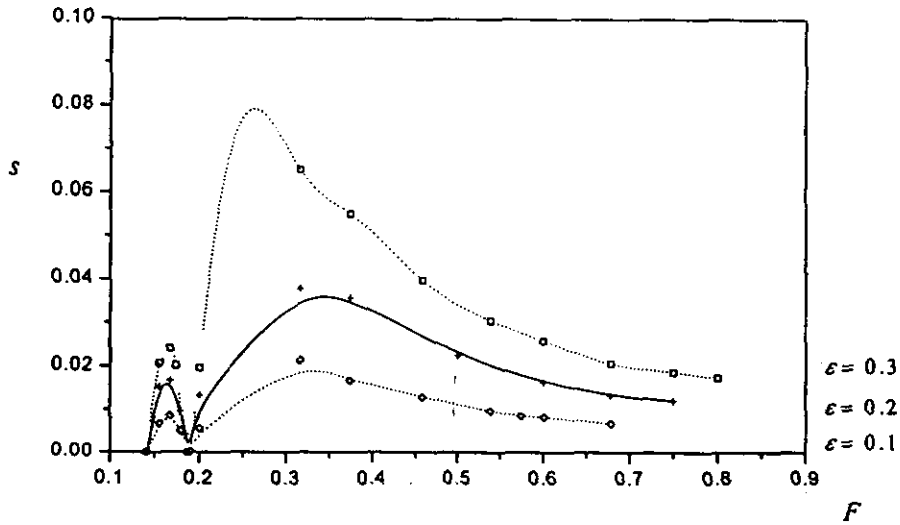

Figure 10(a)

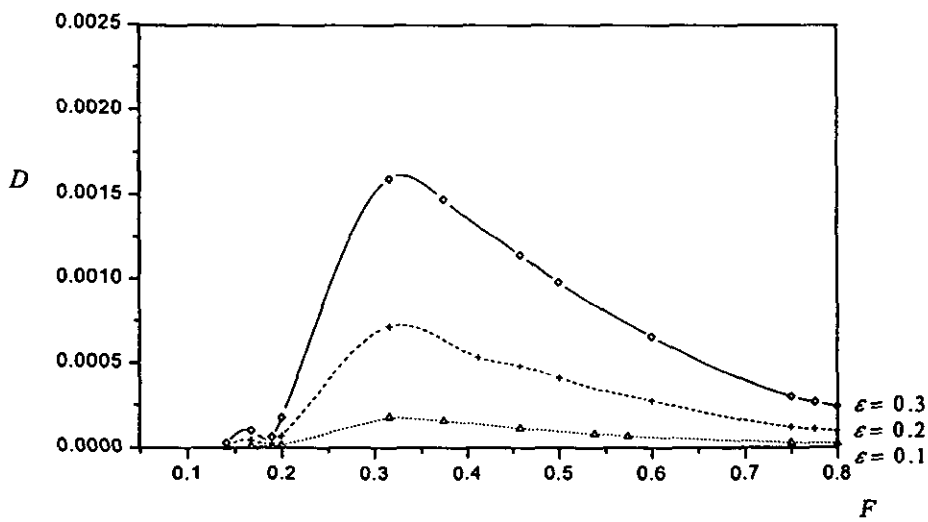

Figure 10(b)

References

[1] H. Lamb. *Hydrodynamics*. Dover Publications, New York, 1945.
[2] L. W. Schwartz. *Nonlinear solution for an applied overpressure on a moving stream*. J. Eng. Math. **12** (1981), 147-156.
[3] C. von Kerczek and N. Salvesen. *Nonlinear free-surface effects-dependence on Froude number*. Proc. 2nd Int. Conf. On Numerical Ship Hydrodynamics, Berkeley, 292–300 (1977).
[4] J. Asavanant and J. M. Vanden-Broeck. *Free surface flows past a surface-piercing object of finite length*. J. Fluid Mech. **273** (1994), 109-124.
[5] J. M. Vanden-Broeck and J. B. Keller. *Surfing on solitary waves*. J. Fluid Mech. **198** (1989), 115-125.
[6] J. Asavanant and M. Maleewong. *Subcritical symmetric gravity-capillary waves due to pressure distributions*, in preparation.
[7] W. Kinnersley, *Exact large amplitude capillary waves on sheets of fluid*. J. Fluid Mech. **77** Part **2** (1976), 229-241.

Jack Asavanant and Montri Maleewong
Department of Mathematics and AVIC Research Center
Faculty of Science
Chulalongkorn University
Bangkok, Thailand
E-mail: ajack@chula.ac.th

Jeongwhan Choi
Department of Mathematics
Korea University, Seoul, Korea